HIGH-VELOCITY, NONRADIATIVE SHOCK EMISSION IN KEPLER'S SUPERNOVA REMNANT

ROBERT A. FESEN[1]
Center for Astrophysics and Space Astronomy, University of Colorado

ROBERT H. BECKER[1]
Department of Physics, University of California at Davis; and
Institute of Geophysics and Planetary Physics, Lawrence Livermore National Laboratory

AND

WILLIAM P. BLAIR[2] AND KNOX S. LONG[2,3]
Department of Physics and Astronomy, The Johns Hopkins University
Received 1988 November 7; accepted 1988 December 6

ABSTRACT

Optical spectra of faint emission seen along the northern limb of Kepler's supernova remnant (SN 1604) show only Hα and Hβ line emissions over the spectral range 4700–7000 Å. The detected Hα emission consists of a broad (FWHM = 40 Å) component and a narrow, unresolved component which, together with the lack of other strong emission lines, indicates the presence of Balmer-dominated or "nonradiative" emission associated with the remnant's high-velocity shocks. This is the first report of nonradiative shock emission in this remnant. Using nonradiative shock models to interpret the width of the broad component and the flux ratio of the broad to narrow components, we estimate a shock velocity of 1670–2800 km s^{-1}. New CCD interference-filter images of the remnant suggest that nonradiative emission is probably present along most of the remnant's northern rim.

Subject headings: nebulae: individual (SN Ophiuchi 1604) — nebulae: supernova remnants — stars: supernovae — shock waves

I. INTRODUCTION

The remnant of Kepler's supernova (SN 1604) appears in the radio and X-rays as a nearly complete limb-brightened shell roughly 3′ in diameter with the brightest emission seen along the northern edge (Gull 1975; White and Long 1983; Matsui et al. 1984; Dickel et al. 1988). The optical emission from the supernova remnant (SNR) covers only a portion of the X-ray and radio shell and consists of a few relatively bright knots along the remnant's northwestern rim with several much fainter knots located near the projected center and along its northeastern limb (Baade 1943; van den Bergh, Marscher, and Terzian 1973; van den Bergh and Kamper 1977). Recent CCD images have revealed additional optical emission in these regions, including a very faint diffuse component extending along most of the northern rim of the remnant (D'Odorico et al. 1986).

Although SN 1604 has been classified as a classic Type I SN (i.e., Type Ia) based on its observed light curve (Baade 1945), a fairly massive progenitor star like that currently suspected in Type Ib and II supernovae is suggested by the interaction of the remnant's expanding shock wave with relatively dense, CNO process–enriched, circumstellar material (van den Bergh, Marscher, and Terzian 1973; White and Long 1983; Hughes and Helfand 1985; Bandiera 1987). The presence of this surrounding high-density interstellar gas despite a location at least 450 pc above the Galactic plane has led to a substantially different optical SNR than that seen in the remnants of the suspected Type Ia supernovae of SN 1006 and SN 1572

(Tycho's SN). Whereas Kepler's high-density optical knots show a variety of emission lines and ionization states characteristic of cooling radiative shocks like those commonly seen in old SNRs (van den Bergh 1980; Dennefeld 1982; Leibowitz and Danziger 1983), the remnants of SN 1006 and Tycho's SN exhibit only faint optical nebulosity whose spectrum is dominated by hydrogen Balmer lines (Kirshner, Winkler, and Chevalier 1987 and references therein).

Balmer-dominated shock emission, often referred to as "nonradiative" emission, is believed to result from the passage of a high-velocity shock through a low-density, partially neutral medium which leads to the production of both broad and narrow hydrogen Balmer emission (Chevalier and Raymond 1978; Chevalier, Kirshner, and Raymond 1980, hereafter CKR). Neutral hydrogen atoms can stream unaffected through the collisionless shock front and can become collisionally excited before becoming collisionally ionized in the postshock plasma, thereby producing a narrow emission line corresponding to the preshock hydrogen's temperature and velocity. Charge exchange with high-velocity protons also produces hydrogen atoms with a thermal energy and velocity distribution comparable to that of the shocked ions, leading to the emission of a broad Balmer line profile corresponding to the postshock temperature and velocity.

Considering the high shock velocity suggested by its X-ray properties (Becker et al. 1980; White and Long 1983; Hughes and Helfand 1985), Kepler's SNR might also exhibit some nonradiative emission if its surrounding medium were partially neutral and of sufficient density to produce detectable Hα flux. Detection of this type of emission would yield a direct measurement of the remnant's current expansion velocity and permit comparison with the observed values in SN 1006 and Tycho's SNR. In this *Letter*, we present optical CCD images and long-slit spectra of the emission filaments in Kepler's SNR

---

[1] Visiting Astronomer, Lick Observatory.

[2] Visiting Astronomer, Las Campanas Observatory operated by the Carnegie Institute of Washington.

[3] Visiting Adjunct Associate, Mount Wilson and Las Campanas Observatories.

which indicate the presence of Balmer-dominated high-velocity shock emission along much of the remnant's northern rim.

II. OBSERVATIONS

Optical images of Kepler's SNR were taken on 1987 April 24 and 25 (UT) with the 2.5 m Du Pont telescope at the Las Campanas Observatory in Chile. A Texas Instruments 800 × 800 pixel CCD was used with an adapted version of the PFUEI focal reducer (Gunn and Westphal 1981) which compressed the f/7.5 telescope beam down to f/2.7. The resultant image scale was $0\rlap{.}''41$ pixel^{-1} with a $5\rlap{.}'3$ field of view. Seeing as measured from star images ranged from $0\rlap{.}''90$ to $1\rlap{.}''1$ (FWHM).

Images were obtained using the following interference filters and exposure times: an Hα filter ($\lambda_0 = 6565$ Å, FWHM = 30 Å; 2000 s), an [O I] filter ($\lambda_0 = 6300$ Å, FWHM = 50 Å; 4000 s), an [O III] filter ($\lambda_0 = 5027$ Å, FWHM = 53 Å; 4000 s), a [S II] filter ($\lambda_0 = 6737$ Å, FWHM = 57 Å; 4000 s), and a red continuum filter ($\lambda_0 = 6100$ Å, FWHM = 130 Å; 2000 s). The Hα filter was broad enough to permit some possible contamination by [N II] $\lambda6583$ emission which is known to be stronger than Hα in many of the remnant's bright filaments, especially if any of this emission is substantially blueshifted. Image data reduction included bias subtraction, dome flat-field corrections, and continuum image alignment and subtraction. The latter step, although unsophisticated, is quite successful in removing stars to first order (see Blair and Long 1988).

Low-dispersion spectra (resolution = 11 Å) were obtained on 1987 July 19 and 20 (UT) using the Cassegrain CCD spectrograph on the 3 m Shane telescope at Lick Observatory. This device consists of a collimator lens, a grism, and a liquid nitrogen–cooled Texas Instruments 800 × 800 pixel CCD. Low-resolution red spectra are collected by inserting a red blaze 600 l mm^{-1} transmission grating along with an order-separating filter (GG 455) into the optical path. An east-west aligned $2\rlap{.}''2 \times 2'$ slit was placed at two positions along the remnant's northern edge as shown on the Hα image in Figure 1 (Plate L2). Slit position 1 is located just north of the brightest optical filaments between knots identified by D'Odorico *et al.*

(1986) as 26–29 and 32, while slit position 2 was located along the northeastern rim, just north of the cluster of knots 53, 55, and 56. Integration times were 3600 s and 4000 s for positions 1 and 2, respectively.

Spectral data reduction included flux calibration through observations of standard stars (BD 33°2642 and BD 40°4032; Stone 1974), wavelength calibration via He-Ne-Hg lamps, and flat-fielding with dome flats. Detected nebular emission was summed over a 15″ distance along the slit at both positions. Sky subtraction was accomplished by averaging strips of sky approximately 15″ on either side of the SNR emission. Because of the crowded star field in this region, faint stellar continua were detected coincident with the Hα emission filaments at both positions. Underlying stellar continuum was subtracted from the Hα emission using average stellar fluxes measured at wavelength regions just shorter and longer than 6563 Å. In the case of slit position 1, this stellar background subtraction produced a noticeable nonzero flux level which was subsequently removed by a spline fit to the background. The resultant unsmoothed spectra are shown in Figure 2. Approximate Hα fluxes are 2.5×10^{-15} and 2.0×10^{-15} ergs cm^{-2} s^{-1} for positions 1 and 2, respectively. Due to variable seeing conditions and large air mass from Lick, our measured absolute fluxes are only reliable to within a factor of 2.

III. RESULTS AND DISCUSSION

The spectra obtained at the two slit positions in Kepler's remnant showed only Hα, Hβ, and possibly weak [N II] $\lambda6583$ line emissions over the wavelength range 4700–7000 Å. The Hα emission line profiles appear to consist of two separate components: a narrow component with instrumental width (FWHM = 11 Å) and a considerably broader component having a width of about 40 Å (FWHM) (see Fig. 2).

The broad Hα emission components detected at both slit positions show comparable line profiles (see Fig. 3). In order to investigate the nature of these broad components, we show in Figure 4 the sum of the two spectra (shifting position 2's Hα emission to coincide with that of position 1 before summing) along with a comparison line profile (Ne I 6598.95 Å), taken on
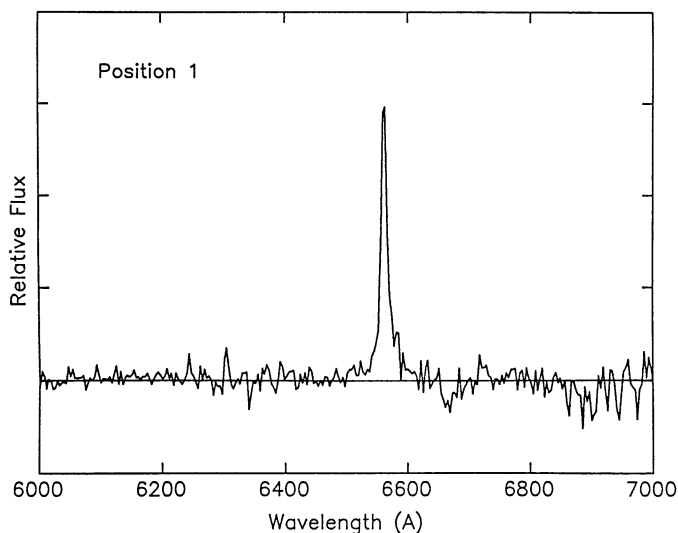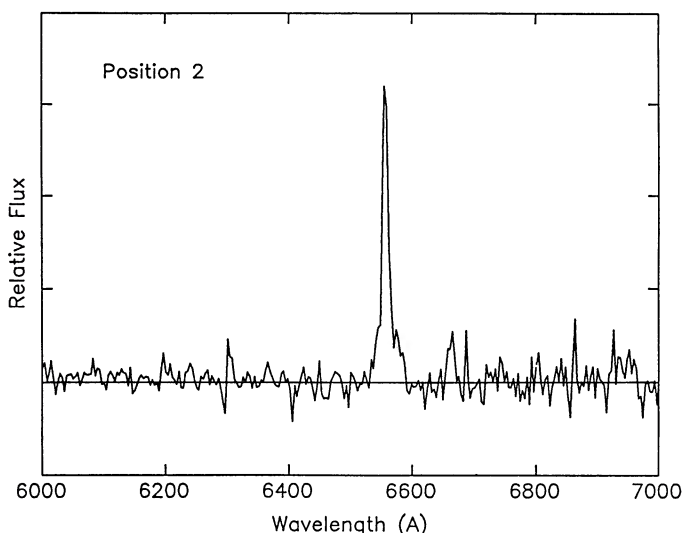

FIG. 2a

FIG. 2b

FIG. 2.—Spectra for slit positions 1 and 2 covering the wavelength range 6000–7000 Å. Hα is the only emission line clearly detected.
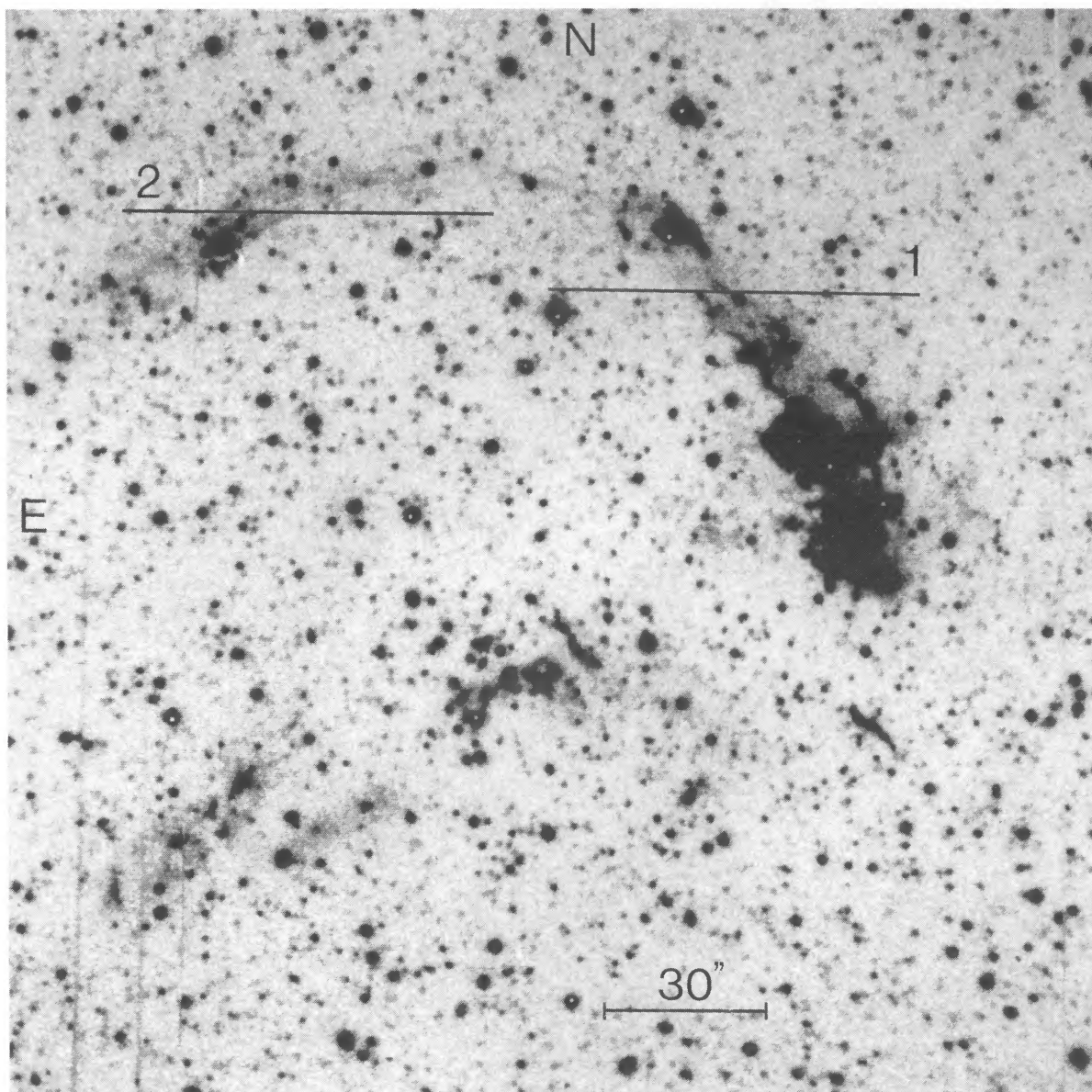
FIG. 1.—Hα image of Kepler's supernova remnant with the two 2″ × 2′ slit positions indicated. Note the presence of faint, diffuse emission along most of the remnant's northern rim.
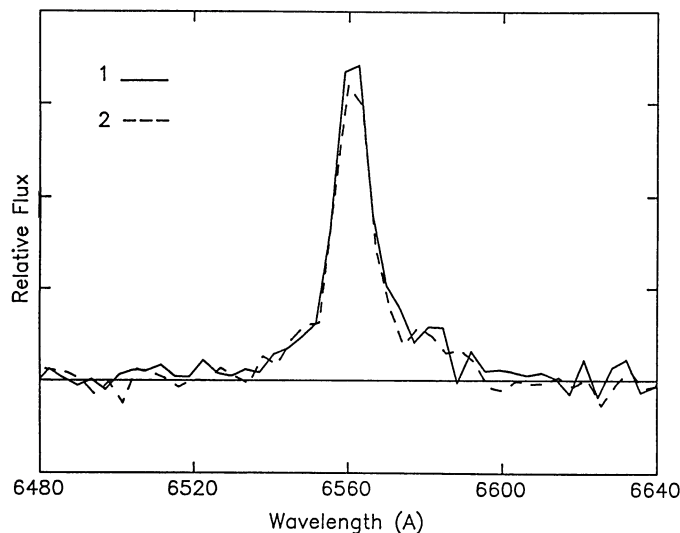
FESEN *et al.* (*see* **338**, L14)

KEPLER'S SUPERNOVA REMNANT

FIG. 3.—Comparison of the Hα emission line profiles observed at positions 1 (*solid line*) and 2 (*dashed line*). The spectrum of position 2 has been shifted so that the two line centers coincide.

the same night as the spectrum for position 2, smoothed to a FWHM of 11 Å, and scaled to the full intensity of the summed Hα emission. No broad component is seen in the comparison line's profile, nor was any similar broad component observed for any other emission-line source observed with the spectrograph on either night. This suggests that the broad component visible at the base of the Hα line profile is not instrumental but intrinsic to the SNR nebulosity. Subtraction of the comparison line (scaled to that of the narrow component) from the summed Hα intensity indicates a flux ratio of the broad component to narrow component (I_b/I_n) of 1.1 ± 0.25.

The lack of other prominent emission lines in these spectra, such as [O I] $\lambda6300$, [S II] $\lambda\lambda6717$, 6731, and [N II] $\lambda\lambda6583$, 6548 which appear strong in the remnant's bright radiative filaments, together with the presence of both broad and narrow Hα emission components suggest that the emission detected at
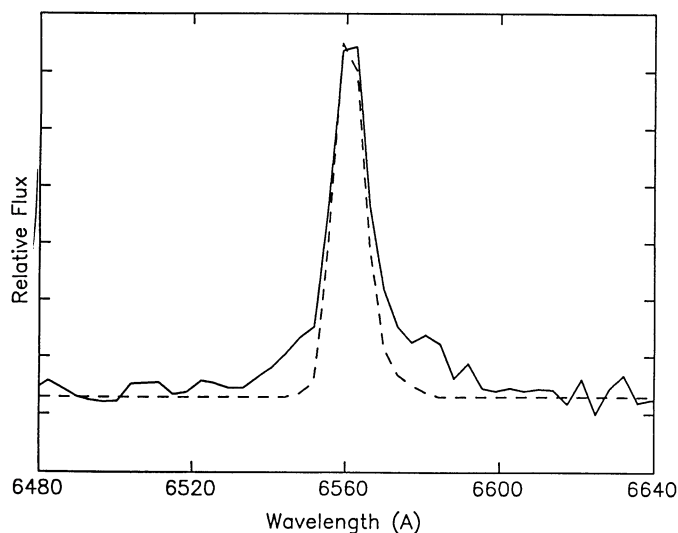

FIG. 4.—Summed Hα line emission detected at both positions (*solid line*) vs. a neon comparison lamp line profile (*dashed line*) having the same relative peak intensity and a FWHM equal to that of the Hα line's narrow component, illustrating the presence of a broad Hα component.

these two positions represents nonradiative shock emission in Kepler's SNR.

While the observed width (FWHM) of Kepler's broad Hα component is comparable to those seen in the nonradiative filaments in Tycho's remnant (Kirshner, Winkler, and Chevalier 1987), an exact measurement is complicated by the possible presence of weak [N II] $\lambda6583$ line emission. As shown in Figures 2 and 3, both spectra show a possible weak feature on the redward side of Hα at a rest wavelength within 2 Å of 6583 Å. Faint [N II] emission has been reported in the nonradiative filaments of the Cygnus Loop (Fesen and Itoh 1985) and suspected in the nonradiative filaments in Tycho's remnant (Kirshner and Chevalier 1978). The presence of this weak [N II] emission decreases the broad component's FWHM by about 2 Å. Assuming [N II] emission is weakly present, the Hα broad component's width (FWHM) is 40 ± 4 Å equivalent to an implied velocity of 1750 ± 200 km s^{-1} after correcting for instrumental resolution.

Both the broad component's line profile and the ratio of narrow to broad component intensities can be used independently to estimate the current shock wave velocity, V_s. Using nonradiative model calculations given in CKR and the observed broad component's line profile, we estimate V_0 the mean gas velocity behind the shock to be 1400 ± 200 km s^{-1} using CKR's model A assumptions (i.e., where only protons are thermalized behind the shock) and 1950 ± 200 km s^{-1} in model B (where the gas is 10% He by number and is completely ionized and thermalized).

Similarly, the ratio of broad to narrow components as a function of V_0 implies a V_0 of 1650 ± 150 km s^{-1} for the model A case where only protons are thermalized (see Fig. 5 of Kirshner, Winkler, and Chevalier 1987). Although a somewhat higher postshock gas velocity would result under the conditions of model B, uncertainties in the electron-ion equilibration behind the shock prevent an exact calculation (CKR).

Because the postshock gas velocity inferred from I_b/I_n is consistent (at least for model A conditions) with the more direct technique using the observed line profiles, we will use the estimates obtained from the broad component profiles. The inferred postshock gas velocities indicate that Kepler's current shock velocity $V_s (= 4/3 V_0)$ lies within the range 1670–2800 km s^{-1} along its northern rim. Because recent radio measurements suggest the remnant is expanding slowest along its radio and X-ray bright northern edge (Dickel *et al.* 1988), Kepler's shock velocity could be higher in other regions.

While the distance to Kepler's SNR is uncertain, most recent estimates place it between 4 and 5 kpc (4.1 ± 0.9 kpc, Braun 1987; 4.2 kpc, Strom 1988; 4.5 kpc, Bandiera 1987; 5.1 kpc, Hughes and Helfand 1985). At a distance of 4.5 kpc, a shock velocity of 1670–2800 km s^{-1} will produce a proper motion of 0″.08–0″.13 yr^{-1}. However, a kinematic distance estimate for the remnant from proper motion measurements is made difficult by the nonradiative emission's diffuse morphology. In contrast to the sharply defined nonradiative filaments seen in both Tycho (Kirshner, Winkler, and Chevalier 1987) and SN 1006 (Long, Blair, and van den Bergh 1988), the nonradiative emission detected at the two slit positions in Kepler's remnant is surprisingly diffuse (see Fig. 1). The presence of faint, diffuse Hα emission all along the remnant's northern rim suggests that nonradiative shock emission is probably not confined to just the two positions studied spectroscopically. This conclusion is strengthened by the fact that none of the diffuse emission along the northern rim was detected in any of the other emission line images.

Wavelength measurements of the narrow Hα components indicate radial velocities of -80 ± 75 km s^{-1} at position 1 and $+50 \pm 75$ km s^{-1} at position 2. Since neutral, low-velocity hydrogen atoms are unaccelerated in the nonradiative shock model, the narrow component's radial velocity is independent of shock front inclination with respect to the plane of the sky. However, both spectra show a small asymmetry in the centroid of the broad components toward the red with a shift of about 4 Å or 200 km s^{-1}. Assuming a shock velocity of 2200 km s^{-1}, this shift suggests an angle of around 5° between the shock normal and the plane of the sky. A similar asymmetry in the broad component was reported in Tycho's nonradiative emission (Kirshner, Winkler, and Chevalier 1987).

Our estimated shock velocity for Kepler's SNR of between 1670 and 2800 km s^{-1} is close to the range 1930–2670 km s^{-1} estimated by Kirshner, Winkler, and Chevalier for Tycho's remnant which is of comparable age. This is in spite of Tycho's SNR having a much lower estimated ambient density of 0.28–0.9 cm^{-3} (CKR; Hamilton, Sarazin, and Szymkowiak 1986; Strom 1988) compared to the 5–10 cm^{-3} estimated for Kepler (White and Long 1983; Matsui *et al.* 1984; Hughes and Helfand 1985; Strom 1988). However, we do not know whether Kepler's and Tycho's SNe had similar initial energies or, as noted above, they involved similar type of SN events. On the other hand, assuming a distance of 2.5 kpc for Tycho's SNR and 4.5 kpc for Kepler's SNR (Strom 1988), these two remnants have quite different average expansion velocities: 7150 km s^{-1} and 5400 km s^{-1} for Tycho's and Kepler's SNRs, respectively.

Estimating Kepler's local preshock H I density using the observed nonradiative emission flux is complicated by the emission's diffuse morphology. If we assume the diffuse morphology offsets the expected increase in surface brightness due to a lack of tangencies along our line of sight, and if we use an optical extinction of $A_v = 3.5$ from previous studies of Kepler's bright radiative filaments (Danziger and Goss 1980; Dennefeld 1982), then the observed Hα flux of 3.5×10^{-6} ergs cm^{-2} s^{-1} sr^{-1} suggests a preshock H I density around 1 cm^{-3}. Although the Hβ line was too poorly detected in our spectra to provide an accurate Hα/Hβ ratio measurement, an Hα/Hβ ratio around 6 seen at both slit positions suggests $A_v \approx 2$. This is considerably less than the $A_v = 3.5$ reported for the remnant's bright filaments, but extinction variations across the remnant have been suspected previously (Dennefeld 1982). In any case,

a lower extinction would imply a lower neutral preshock density.

Our CCD images, like those of D'Odorico *et al.* (1986), indicate the presence of considerable diffuse Hα emission throughout the remnant (see Fig. 5 [Pls. L3–L4]). As shown in the continuum-subtracted Hα image (Fig. 5*b*) which extends farther to the west than D'Odorico *et al.*'s images, we detected faint, diffuse Hα emission to the west of the bright radiative filaments. This faint emission is roughly coincident with the western radio "bulge" (see Dickel *et al.* 1988). Also, considerably more diffuse emission is seen surrounding the centrally located knots. A lack of detectable [S II], [O I], and [O III] emission in these diffuse emission regions suggests that the faint, diffuse, nonradiative emission we have found along the northern limb may be widespread in Kepler's SNR.

Because these pictures were taken under excellent seeing and transparency conditions, we have also detected some additional faint knots of emission beyond those identified by D'Odorico *et al.* (1986). Most of these knots are seen at a very low level on our [S II] image, but some are not. This could be due to the limiting sensitivity of the exposures, but it also raises the possibility that some knotty emission may also be nonradiative.

In summary, we have successfully detected nonradiative shock emission in Kepler's SNR. This nonradiative emission exhibits a diffuse morphology in contrast to the sharp filaments observed in the remnant of SN 1006 and Tycho's SNR. Nonradiative shock emission in a young remnant which also exhibits bright radiative shock emission raises questions about classification schemes of young SNRs based upon the presence or absence of nonradiative filaments (van den Bergh 1988). More importantly, it shows that it is possible to directly measure interstellar shock velocities in bright radiative SNRs so long as there is sufficient surrounding neutral gas. This offers the possibility of studying the dynamical evolution of young SNRs by comparing their shock front's velocity and expansion radius with those of the ejecta.

REFERENCES

Baade, W. 1943, *Ap. J.*, **97**, 119.
———. 1945, *Ap. J.*, **102**, 309.
Bandiera, R. 1987, *Ap. J.*, **319**, 885.
Becker, R. H., Boldt, E. A., Holt, S. S., Serlemitsos, P. J., and White, N. E. 1980, *Ap. J. (Letters)*, **237**, L77.
Blair, W. P., and Long, K. S. 1988, *Pub. A.S.P.*, **100**, 461.
Braun, R. 1987, *Astr. Ap.*, **171**, 233.
Chevalier, R. A., Kirshner, R. P., and Raymond, J. C. 1980, *Ap. J.*, **235**, 186 (CKR).
Chevalier, R. A., and Raymond, J. C. 1978, *Ap. J. (Letters)*, **225**, L27.
Danziger, I. J., and Goss, W. M. 1980, *M.N.R.A.S.*, **190**, 49P.
Dennefeld, M. 1982, *Astr. Ap.*, **112**, 215.
Dickel, J. R., Sault, R., Arendt, R. G., Matsui, Y., and Korista, K. T. 1988, *Ap. J.*, **330**, 254.
D'Odorico, S., Bandiera, R., Danziger, J., and Focardi, P. 1986, *A.J.*, **91**, 1382.
Fesen, R. A., and Itoh, H. 1985, *Ap. J.*, **295**, 43.
Gull, S. F. 1975, *M.N.R.A.S.*, **171**, 237.

Gunn, J. E., and Westphal, J. A. 1981, *Proc. SPIE*, **290**, 16.
Hamilton, A. J. S., Sarazin, C. L., and Szymkowiak, A. E. 1986, *Ap. J.*, **300**, 713.
Hughes, J. P., and Helfand, D. J. 1985, *Ap. J.*, **291**, 544.
Kirshner, R. P., and Chevalier, R. A. 1978, *Astr. Ap.*, **67**, 267.
Kirshner, R. P., Winkler, P. F., and Chevalier, R. A. 1987, *Ap. J. (Letters)*, **315**, L135.
Leibowitz, E. M., and Danziger, I. J. 1983, *M.N.R.A.S.*, **204**, 273.
Long, K. S., Blair, W. P., and van den Bergh, S. 1988, *Ap. J.*, **333**, 749.
Matsui, Y., Long, K. S., Dickel, J. R., and Greisen, E. W. 1984, *Ap. J.*, **287**, 295.
Stone, R. P. S. 1974, *Ap. J.*, **193**, 135.
Strom, R. G. 1988, *M.N.R.A.S.*, **230**, 331.
van den Bergh, S. 1980, *Astr. Ap.*, **86**, 155.
———. 1988, *Ap. J.*, **327**, 156.
van den Bergh, S., and Kamper, K. W. 1977, *Ap. J.*, **218**, 617.
van den Bergh, S., Marscher, A. P., and Terzian, Y. 1973, *Ap. J. Suppl.*, **26**, 19.
White, R. L., and Long, K. S. 1983, *Ap. J.*, **264**, 196.

ROBERT H. BECKER: Physics Department, University of California, Davis, CA   95616

WILLIAM P. BLAIR and KNOX S. LONG: Department of Physics and Astronomy, 170 Rowland Hall, The Johns Hopkins University, Baltimore, MD   21218

ROBERT A. FESEN: Center for Astrophysics and Space Astronomy, Campus Box 391, University of Colorado, Boulder, CO   80309
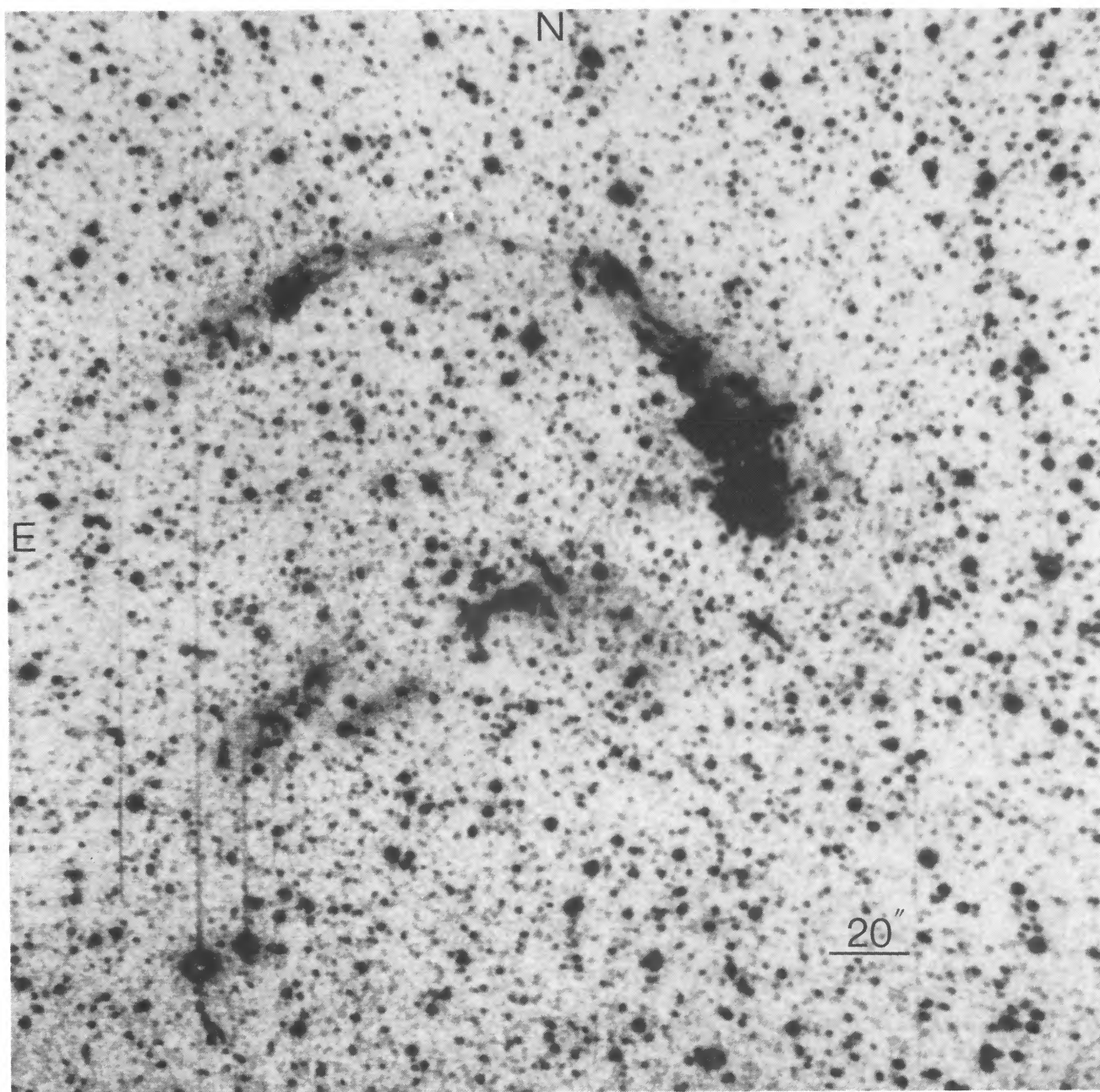
FIG. 5a

FIG. 5.—(a) Deep Hα image and (b) Hα minus 6100 Å continuum image of Kepler's supernova remnant. In addition to the detection of Hα emission along the remnant's northern rim and surrounding its central emission knots, these images indicate the presence of faint, diffuse emission west of the bright northwestern emission knots at a position that coincides with the remnant's western radio emission "bulge." North is at the top; east, to the left.

FESEN et al. (see 338, L16)

FIG. 5b

FESEN *et al.* (*see* **338**, L16)